Development of a Novel Pt_3V Alloy Electrocatalyst for Highly Efficient and Durable Industrial Hydrogen Evolution Reaction in Acid Environment

Yumin Da, Rui Jiang, Zhangliu Tian, Ganwen Chen, Yukun Xiao, Jinfeng Zhang, Shibo Xi, Yida Deng, Wei Chen, Xiaopeng Han*, Wenbin Hu*

Abstract

Alloying platinum with early transition metals is a promising approach to optimize the adsorption behaviors of catalysts. Nevertheless, the large negative redox potential between early transition metals and Pt hinders the fabrication of such alloys. Herein, a strategy combining the thermal shock technique with electrochemical activation to prepare Pt_3V alloy as a hydrogen evolution reaction catalyst is reported for the first time. Electrochemical tests show that the as-prepared catalyst exhibits exceptional catalytic activity and durability in 0.5 m H_2SO_4, surpassing the state-of-the-art 20 wt.% Pt/C. The catalyst can maintain its activity after 100 h tests without evident decay under the current density of 500 mA cm^{-2}. Theoretical calculations demonstrate that the optimized hydrogen absorption and high vacancy formation energy of Pt_3V contributes to the enhanced electrocatalytic activity and stability. This work may spur future research for other Pt-based early transition metal alloy catalysts for electrocatalysis.

1 Introduction

Hydrogen energy with the advantages of environmental friendliness and high energy density is regarded as an ideal alternative to nonrenewable fossil fuels.[1] Electrochemical water splitting is considered as sustainable technique to produce clean hydrogen. However, owing to the sluggish hydrogen evolution reaction (HER) kinetics, developing electrocatalysts with high activity and superior stability is fundamental to lower the reaction barrier and accelerate the reaction process.[2] To date, Pt-based materials are recognized as benchmark catalysts for HER.[3] Despite extensive research has been conducted on Pt-based electrocatalysts, few reports about Pt-based precious metals can simultaneously meet the activity and stability for HER, especially at large current density, limiting their large-scale commercialization.[2] Hence, conducting more in-depth research to fabricate cost-effective and highly efficient electrocatalysts is vital to realize large-scale applications.

Despite various Pt-based alloys have been reported to be promising to serve as HER electrocatalysts,[4] limited research has been conducted on alloying with early transition metals from group 3 to group 7 (V, Mo, W, etc.) owing to the large negative redox potential to reduce the transition metal cation precursor into the zero-valent metal.[5] Vanadium is a typical early transition metal with multiple valence state, which is promising to optimize the catalytic activity of the host material attributed to the adjustable electronic structure.[6] Moreover, it is feasible to induce synergistic interactions between the heteroatom and host.[7] In addition, the low price and abundant reserves make it

applicable for commercialization. V-based materials have been widely investigated in the electrocatalytic field owing to the unique characteristics, including Ni-VC,[8] NiVRu-LDH,[1] and V_8C_7.[9] However, few reports examined the Pt–V alloys,[10] owing to the requirements of oxygen-free environment and strong reducing agents in traditional wet-chemistry methods.[11]

Recently, thermal shock technique (TST) was reported to prepare well-dispersed nanoparticles on conducive substrates without agglomeration, which is feasible to fabricate various immiscible components with rapid heating and quenching.[12] Moreover, electrochemical activation (including cyclic voltammetry (CV) treatment, linear sweep voltammetry (LSV) etching) is reported as an efficient approach to synthesize materials with controllable structure and outstanding performance. For instance, Sun synthesized a series of Fe_xV_{1-x} composite working as OER electrocatalyst for the first time.[13] Specifically, the VCl_3 and $FeCl_3$ precursors were used to prepare core-shell structure VO_2/V_2O_5@FeOOH. Subsequently, LSV was conducted on the sample in 1 m KOH to remove the VO_2/V_2O_5, leaving the V^{3+} doped FeOOH shell and forming the hollow $Fe_{0.5}V_{0.5}$ spheres. X-ray photoelectron spectroscopy (XPS) verified the successful removal of V^{4+} and V^{5+} after OER process. Electrochemical tests reveal the low overpotential, high current density, and small Tafel slope of the as-prepared sample. Moreover, a similar work was reported that $Co_2(OH)_3Cl/VO_x$ composite was prepared, followed by CV treatment to remove the VO_x.[14] Simultaneously, $Co_2(OH)_3Cl$ was in situ transformed to CoOOH with abundant surface oxygen vacancies, which is critical to tailor the intrinsic OER activity of CoOOH. Besides, Zhao proposed to use V as both sacrificial agent and dopant to optimize the electronic structure and reconstruct the active phases of V-Ni_2P/NF-AC.[7] Owing to the partially self-dissolution of V, the electrochemical surface area with abundant active sites can be enlarged. Experimental results show that the as-synthesized catalyst owns low overpotential and excellent stability. Combined with theoretical calculations, V dopants can facilitate the kinetics for the adsorption of *OH and deprotonation of *OOH, as well as lowering the energy barrier of the rate-determining step. To this end, in-depth research have to be conducted on the phase reconstruction and surface modification to identify the origin of the HER activity.

Pt_3V alloy have been applied as catalysts toward methanol oxidation[11] and propane dehydrogenation,[11] etc. However, no research about the HER application of Pt_3V are reported till now. In addition, owing to the requirements of oxygen-free atmosphere or reducing agent, Pt–V alloys are difficult to synthesize.[11] Integrating the characteristics of ultrafast thermal shock technique and the facile electrochemical activation, we proposed to synthesize Pt_3V alloy as HER catalyst for the first time. Electrochemical measurements reveal that the as-prepared catalyst exhibits exceptional catalytic activity and stability both in 0.5 m H_2SO_4 and 1 m KOH, outperforming 20 wt.% Pt/C and most of reported materials. The catalyst can maintain the activity without evident decay after 100 h tests under the current density of 500 mA cm^{-2} in acid. Density functional theory

(DFT) calculations reveal that the optimized hydrogen adsorption strength and the high vacancy formation energy leads to the improved HER activity and superior stability of Pt_3V, respectively.

2 Results and Discussions

As illustrated in **Figure** 1a, the carbon cloth coated with the precursors (VCl_3, H_2PtCl_6) was immersed in the liquid nitrogen, followed by the thermal shock technique with direct current (DC) power supply to fabricate p-Pt_3V. Subsequently, anodic activation (Figure S1, Supporting Information) was used to etch the surface vanadium atoms under the applied potential owing to the lower stability of V compared to that of Pt, and the sample obtained after 1 h activation was denoted as a-Pt_3V. As shown in Figure 1b, X-ray powder diffraction (XRD) patterns present that p-Pt_3V is composed of Pt_3V and $VC_{0.85}$. As evidenced from the positive shift of the main peak compared to Pt owing to the smaller lattice constant of V relative to Pt atom (inset in Figure 1b), Pt_3V phase can be determined. $VC_{0.85}$ was gradually removed during the activation process owing to the high potential, and no signal of $VC_{0.85}$ can be detected in a-Pt_3V, suggesting the successful preparation of pure Pt_3V phase. Scanning electron microscopy (SEM) images were collected to investigate the morphology of the samples. As displayed in Figures S2 and S3 (Supporting Information), p-Pt_3V was composed of $Pt_3V/VC_{0.85}$ composites. However, the morphology of Pt_3V nanoparticles was maintained after the anodic activation, while $VC_{0.85}$ was removed for a-Pt_3V (Figures S4 and S5, Supporting Information). Besides, the crystal lattices with spacings of 2.22 and 2.38 Å presented in the high resolution transmission electron microscopy (HRTEM) images (Figure 1c) of the pristine samples correspond to the (112) and (111) planes of Pt_3V and $VC_{0.85}$, respectively, confirming the formation of $Pt_3V/VC_{0.85}$ composite in p-Pt_3V. Differently, as shown in Figure 1d, TEM images of a-Pt_3V show that only Pt_3V can be observed, and $VC_{0.85}$ were removed successfully, which is in accordance with XRD results. Energy dispersive spectroscopy (EDS) mapping of Pt and V depicts the homogeneous distribution of these elements in p-Pt_3V and a-Pt_3V (Figure 1e,f). High-angle annular dark field (HAADF-STEM) was adopted to directly observe the atomic configurations of a-Pt_3V. As displayed in Figure 1g, the bright spots can be assigned to Pt atoms in the structure, attributed to the different contrasts between Pt and V atoms in the inner part. The enlargement figure reveals the spaced arrangement of atoms as evidenced by the dark V atoms and bright Pt atoms in Figure 1h. Moreover, the intensity profile displays the formation of Pt_3V alloy (Figure 1i). In addition, bright dots can be observed on the outside layers of a-Pt_3V, which belongs to Pt atoms. Thus, the structure can be determined to be core–shell.

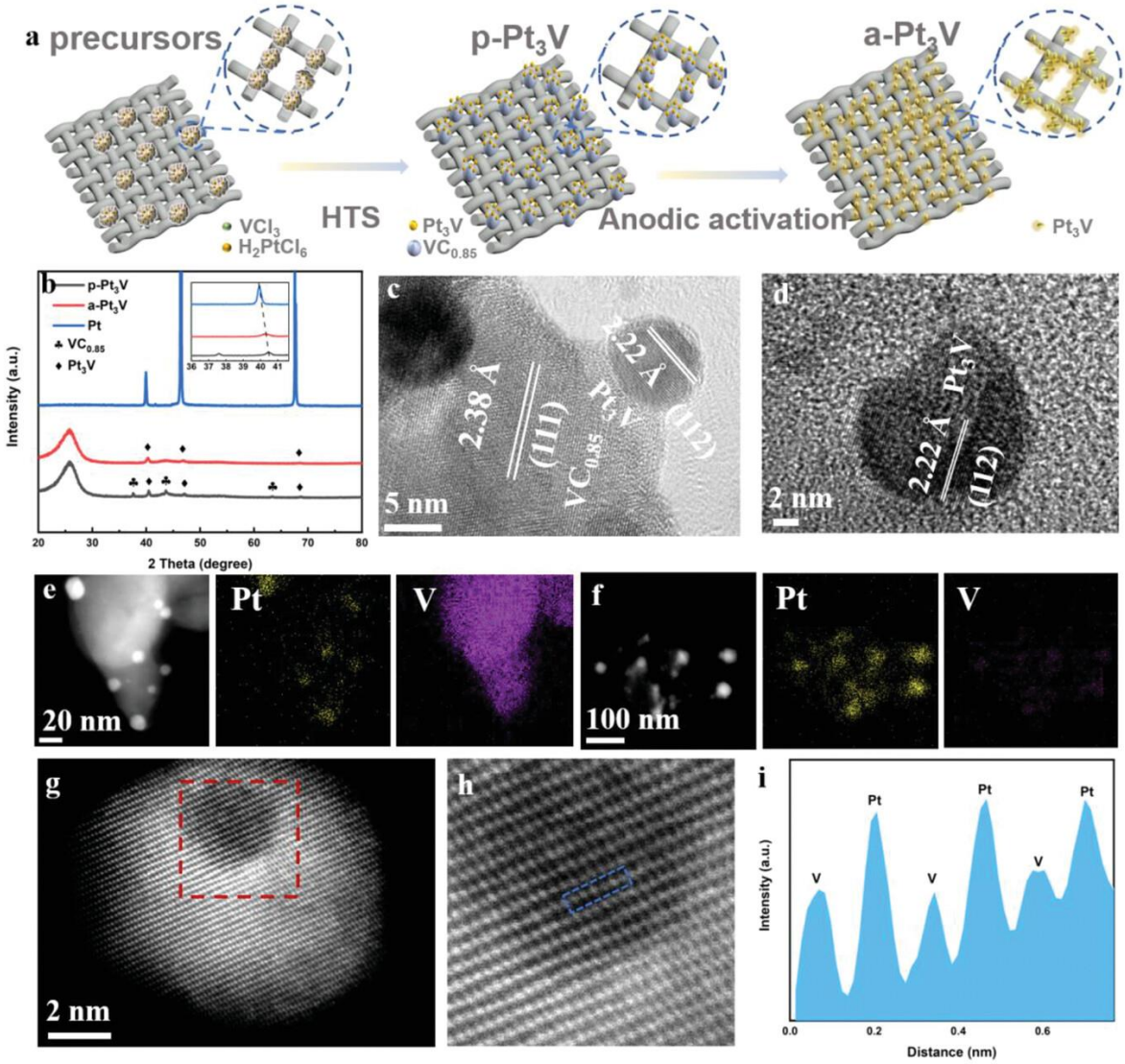

Figure 1 a) Synthetic processes of p-Pt_3V and a-Pt_3V, b) XRD pattern of p-Pt_3V, a-Pt_3V, and 20 wt.% Pt/C, inset: enlargement of XRD, c) HRTEM of p-Pt_3V, d) HRTEM of a-Pt_3V, e) EDS mapping of p-Pt_3V, f) EDS mapping of a-Pt_3V, g) HAADF-STEM image of a-Pt_3V, h) enlargement of (g), i) line intensity profile of a-Pt_3V.

XPS was conducted to investigate the chemical properties of the samples. As shown in Figure S6a (Supporting Information), the Pt 4f spectrum of p-Pt_3V can be deconvoluted into four peaks located at 71.3, 73.1, 74.7, and 76.4 eV, respectively, demonstrating the existence of Pt^0 and Pt^{2+}.[15] For the pristine a-Pt_3V, the intensity of V is very weak, while that of Pt is stronger (**Figure** 2a). The Pt 4f spectrum of a-Pt_3V can be deconvoluted into four peaks located at 71.5, 72.9, 74.9, and 76.3 eV, respectively, confirming that the existence of metallic Pt on the surface of a-Pt_3V. Besides, V 2p XPS spectra (Figure S6b, Supporting Information) display that vanadium owns abundant valence state in p-Pt_3V. The peaks positioned at 514.0, 516.1, 517.3, and 518.5 eV correspond to V^{2+}, V^{3+}, V^{4+}, and V^{5+}, respectively.[1, 2, 13] However, the intensity of V in a-Pt_3V is significantly weaker than p-Pt_3V, manifesting that the leaching of partial vanadium atoms from the outer surface

(Figure 2b). In order to confirm the structure of a-Pt_3V, we conduct XPS etching with Ar plasma. As shown in Figure 2a,b, for the pristine a-Pt_3V, the intensity of V is very weak, while that of Pt is strong. It suggests that the surface of a-Pt_3V is mainly composed of Pt. After 1 keV Ar ion etching for 300, 600, and 900 s, the characteristic peaks of V appear, while the peak of Pt shifts to lower binding energy. It suggests that the electron transfer from V to Pt, indicating Pt_3V alloy exists in the sub-surface. Thus, the a-Pt_3V is core–shell structure with Pt_3V core and Pt shell.

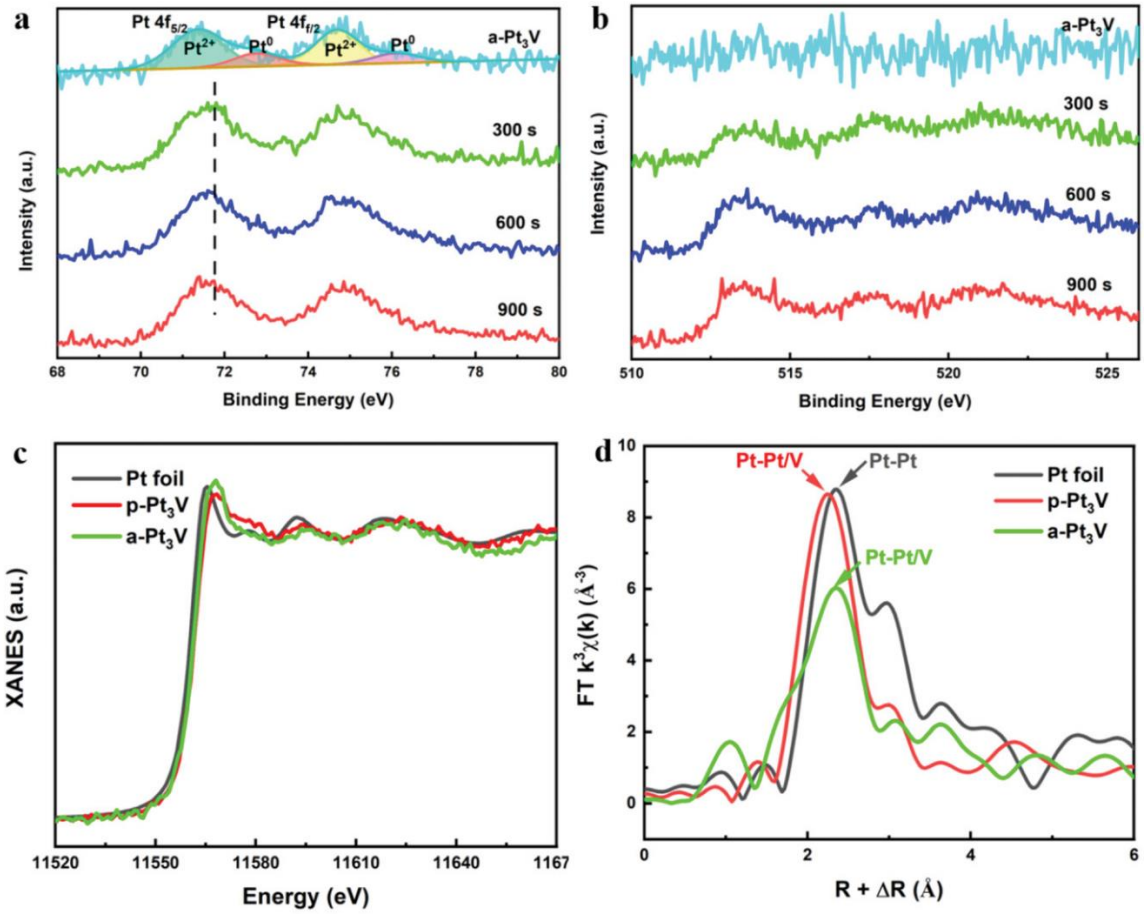

Figure 2 XPS spectra of a) Pt 4f, b) V 2p of a-Pt_3V and a-Pt_3V with Ar etching for 300, 600, and 900 s, c) XANES spectra, d) Pt L_3-edge EXAFS spectra of p-Pt_3V and a-Pt_3V.

Moreover, X-ray absorption spectroscopy was conducted to investigate the electronic structure of the as-prepared samples. As shown in Figure 2c, the rising edge of a-Pt_3V and p-Pt_3V is lower than that of Pt foil, indicating Pt in the former samples are in oxidation states. The higher white-line intensity of a-Pt_3V derived from 2*p* to 5*d* orbital transition suggests more unoccupied orbital of Pt atoms in a-Pt_3V (Figure S7, Supporting Information). Extended X-ray absorption fine structure (EXAFS) spectra at Pt L_3-edge suggest that p-Pt_3V and a-Pt_3V exhibit dominant peaks around 2.3 Å corresponding to Pt–Pt/V scattering paths, confirming the formation of Pt_3V (Figure 2d).[11] Notably, the larger Pt–Pt/V bond in a-Pt_3V (2.34 Å) with respect to that of p-Pt_3V (2.24 Å) is resulted from the

removal of V atoms with smaller atomic radius in comparison to Pt atoms, which is in consistent with XRD results.

As mentioned above, anodic activation was conducted on p-Pt_3V under the certain potential to prepare a-Pt_3V. First, the electrocatalytic measurements of the catalysts were performed in the acid electrolytes. Impressively, as illustrated in the LSV curves, the overpotential of a-Pt_3V (20 mV) is the smallest compared to that of p-Pt_3V (110 mV) and 20 wt.% Pt/C (30 mV) at the current density of 10 mA cm^{-2}, indicating the significantly improved HER activity after the activation (**Figure** 3a). In addition, compared with the other two samples, a-Pt_3V needs only 300 mV to reach current density of 1 A cm^{-2}, which is suitable for industrialization. Figure 3b displays the comparison of the overpotential of the as-synthesized samples under the current density of 10, 50, and 100 mA cm^{-2}. Note that a-Pt_3V only needs 20 and 79 mV to deliver the current density of 10 and 100 mA cm^{-2}, respectively, which is much lower than that of 20 wt.% Pt/C (30 and 235 mV). Additionally, the Tafel slope of a-Pt_3V is only 36 mV dec^{-1}, outperforming that of p-Pt_3V (94 mV dec^{-1}) and 20 wt.% Pt/C (43 mV dec^{-1}; Figure 3c). The smaller Tafel slope suggests the faster HER reaction kinetics. Furthermore, electrochemical impedance spectroscopy (EIS) measurements indicate the smallest charge transfer resistance of a-Pt_3V, which is conducive to facilitate the electron transfer (Figure S8, Supporting Information). Hydrogen binding energy is a descriptor for HER, which can be determined from hydrogen desorption potential (E_{eds}) by CV, As shown in Figure S9 (Supporting Information), E_{eds} of a-Pt_3V appears at 0.09 V, which is lower than that of Pt/C (0.10 V), suggesting that the hydrogen binding energy of a-Pt_3V is the most preferred for HER. Importantly, long-term stability under large current densities is a critical parameter to determine the practical application prospect of the catalysts. We conducted the stability tests of a-Pt_3V under the current density of 10, 100, 300, 500, and 10 mA cm^{-2} for total 50 hours. It reveals that only negligible increase of the overpotential can be observed (inset in Figure 3d). Moreover, it shows exceptional stability after continuous work for 100 h at 500 mA cm^{-2} without evident decay, demonstrating the outstanding electrochemical durability of the a-Pt_3V and the industrial potential of the catalyst (Figure 3d). Figure S10 (Supporting Information) demonstrates that the phase structure remains unchanged. Figure S11 (Supporting Information) shows the uniform distribution of Pt and V atoms after stability tests. Figure S12 (Supporting Information) confirms the existence of Pt_3V. To evaluate the durability of a-Pt_3V, the accelerated degradation tests were conducted for 5000 cycles CV scanning. It reveals negligible loss in HER activity, demonstrating the outstanding durability of the catalyst (Figure 3e). Moreover, Figure 3f compares the overpotentials of representative HER catalysts under the current density of 100 mA cm^{-2}. The a-Pt_3V synthesized in this work exhibits the lowest overpotential with respect to the catalysts reported in the literature (Table S1, Supporting Information). In addition, HER activity of the samples was tested in base (1 m KOH). As illustrated in Figure S13 (Supporting Information), the overpotentials of p-Pt_3V, a-Pt_3V, and

20 wt.% Pt/C are 40, 25, and 70 mV, respectively, manifesting the superior HER activity of a-Pt_3V. The smallest Tafel slope of a-Pt_3V indicates the fastest HER reaction kinetics. Figure S14 (Supporting Information) demonstrates a-Pt_3V can maintain the stability under current density of 300 mA cm^{-2} for 100 h without evident decay. All the above-mentioned results show that a-Pt_3V owns superior activity and stability in both acid and base.

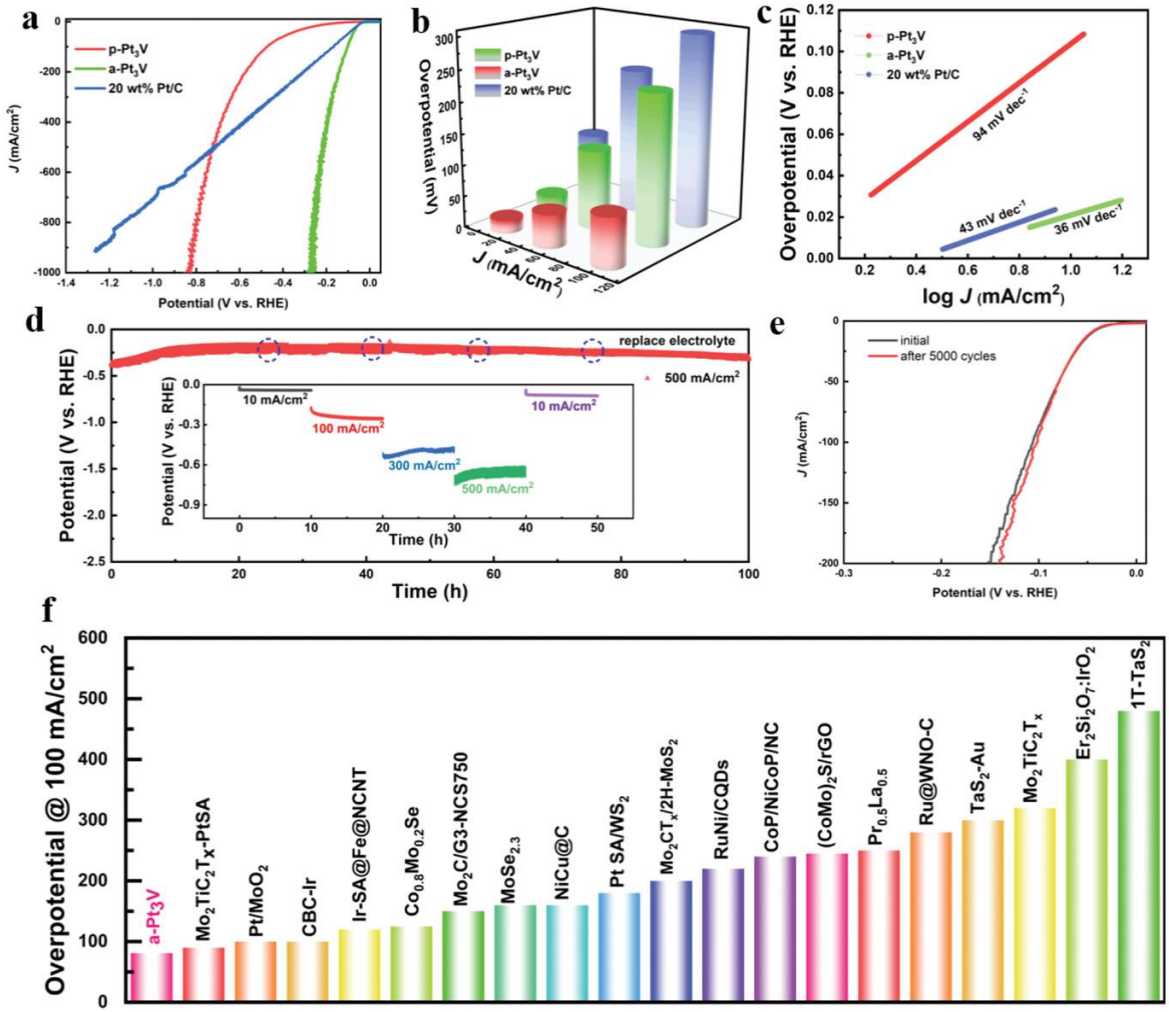

Figure 3 a) LSV curves, b) comparison of the overpotential of a-Pt_3V, p-Pt_3V, and 20 wt.% Pt/C under the current density of 10, 50, and 100 mA cm^{-2}, c) Tafel slope of a-Pt_3V, p-Pt_3V, and 20 wt.% Pt/C, d) stability tests of Pt_3V under the current density of 500 mA cm^{-2}, insert: stability tests of a-Pt_3V under the current density of 10, 100, 300, 500, and 10 mA cm^{-2}, e) LSV curves of a-Pt_3V before and after durability tests, f) comparison of the overpotential of a-Pt_3V with catalysts in literatures.

We performed ultraviolet photoelectron spectroscopy (UPS) to estimate the d-band center. The UPS spectra for a-Pt_3V, Pt, and p-Pt_3V are shown in **Figure** 4a. The work function of a-Pt_3V is lower than that of p-Pt_3V and Pt, suggesting the faster electron transfer ability of a-Pt_3V, thus leading to the enhanced HER activity. We further performed DFT calculations to clarify the origin of the enhanced electrocatalytic activity and stability of the as-prepared catalyst. We first constructed the models as shown in

Figure 4b,c. The structure of a-Pt_3V is composed of Pt skin and Pt_3V core. Differential charge density map illustrates that the electron transfer from V to Pt atoms, which is consistent with XPS results (Figure 4d). Besides, the projected d-density of states (PDOS) of Pt and a-Pt_3V were calculated. The d-band center is considered as a descriptor to evaluate the adsorption strength. As displayed in Figure 4e, the introduction of V leads to the negative shift of d-band center in comparison to Pt. It indicates an elevated occupation of antibonding states between a-Pt_3V and adsorbate, which is conducive to weaken hydrogen adsorption and improve HER kinetics. The HER process involves *H adsorption, and H_2 desorption through two coupled H^+/e^- steps. The Gibbs free energy (ΔG_{H^*}) is regarded as a descriptor of HER activity, and the close-to-zero ΔG_{H^*} is the optimum value for the adsorption and desorption processes. As displayed in Figure 4f and Figure S15 (Supporting Information), the ΔG_{H^*} value of a-Pt_3V is 0.26 eV, which is even lower than that of Pt (111) (−0.30 eV). It reflects that the formation of a-Pt_3V alloy will facilitate HER activity. Besides, the electronic structure of Pt (111) and a-Pt_3V was calculated. As displayed in Figure 4g, it exhibits a high correlation between *H adsorption energy with the d-band center of Pt sites with an R^2 of 0.87, indicating V-dopant can decrease the 4d state of Pt atoms towards lower energy level and thus *H adsorption. Accordingly, the decreased *H adsorption on Pt sites can promote HER process. Moreover, sub-surface V atoms will donate electrons to the neighboring Pt atoms owning to the lower electronegativity of V atoms, leading to the downshift d-band center of Pt atoms in a-Pt_3V compared to pure Pt.[16] It would weaken the hydrogen adsorption and thus accelerate HER kinetics.

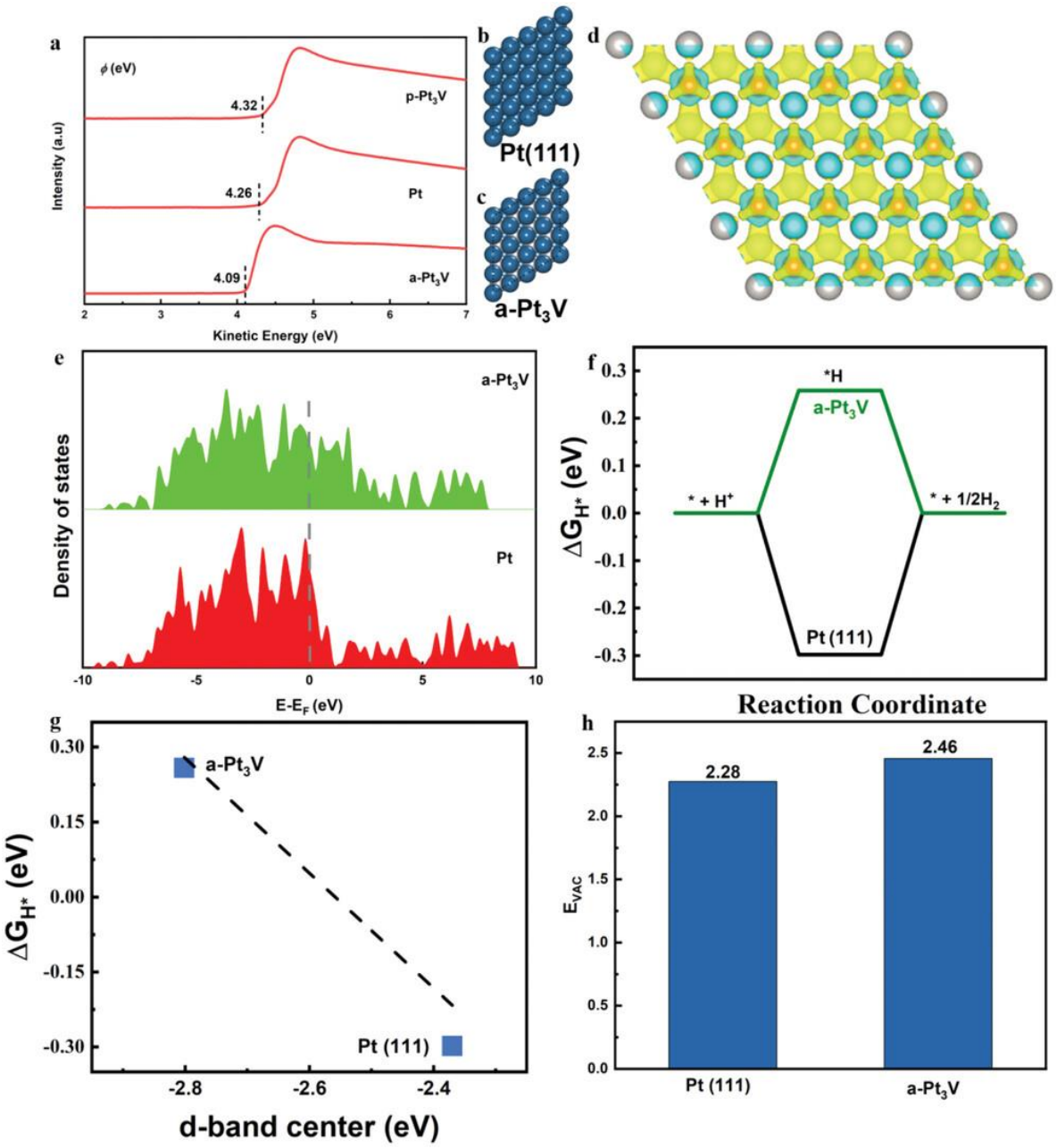

Figure 4 a) UPS spectra for a-Pt_3V, p-Pt_3V, and Pt. b) Top views of Pt (111), and c) a-Pt_3V. The blue and grey balls represent Pt and V atoms, respectively, d) Differential charge density of a-Pt_3V. Cyan and yellow areas represent charge accumulation and depletion, respectively. e) PDOS of surface Pt atoms for Pt (111) and Pt_3V. f) the Gibbs free energy profile on Pt sites, g) the correlation between the d-band center of active Pt atoms and corresponding *H adsorption, h) the dissolution potential of Pt atom from Pt (111) and Pt_3V.

The vacancy formation energy (E_{vac}) of the outermost is regarded as a descriptor to evaluate the durability of Pt-based electrocatalysts.[15, 17] The larger E_{vac} value indicates the higher dissolution potential of atoms, endowing larger hindrance to dissolve the atoms. Figure 4h demonstrates that the E_{vac} value of a-Pt_3V is 2.46 eV, respectively,

surpassing that of Pt (111). It evidences the higher stability of a-Pt_3V in comparison to Pt. The above-mentioned results manifest that the weakened adsorption energy of intermediates on a-Pt_3V, thus signifying enhanced HER activity. In sum, the formation of a-Pt_3V alloy can improve the catalytic activity and stability of Pt catalysts via strong V-Pt bonding effect.

3 Conclusion

Thermal shock combined with anodic activation strategy was utilized to prepare novel Pt_3V catalyst toward electrocatalytic HER for the first time. Electrochemical measurements demonstrate that the HER activity of the Pt_3V is superior to 20 wt.% Pt/C. In addition, outstanding stability can be obtained that the activity can be maintained after 100 h tests under large current density (500 mA cm^{-2}). DFT calculations reveal that the increased vacancy formation energy of Pt_3V is correlated with the stability, and the weakened adsorption energy of intermediates results in the superior activity. This method is promising to synthesize other Pt-based early transition metal alloys.

Acknowledgements

Y.M.D. and R.J. contributed equally to the work. This work was supported by the National Natural Science Foundation of China (52122107 and 51972224), the National Research Foundation, Singapore, and A*STAR (Agency for Science, Technology and Research) under its LCER FI program Award No U2102d2002. X.H. also thanks the Haihe Laboratory of Sustainable Chemical Transformations for financial support.

References

[1] a) D. Wang, Q. Li, C. Han, Q. Lu, Z. Xing, X. Yang,Nat. Commun.2019, 10, 3899; b) Y. Shi, Z. R. Ma, Y. Y. Xiao, Y. C. Yin, W. M. Huang,Z. C. Huang, Y. Z. Zheng, F. Y. Mu, R. Huang, G. Y. Shi, Y. Y. Sun,X. H. Xia, W. Chen, Nat. Commun. 2021, 12, 3021; c) R. Jiang, Y. Da,Z. Chen, X. Cui, X. Han, H. Ke, Y. Liu, Y. Chen, Y. Deng, W. Hu, Adv.Energy Mater. 2022, 12, 2101092.

[2] a) K. L. Zhou, Z. Wang, C. B. Han, X. Ke, C. Wang, Y. Jin, Q. Zhang,J. Liu, H. Wang, H. Yan, Nat. Commun. 2021, 12, 3783; b) Z. Chen,H. Qing, R. Wang, R. Wu, Energy Environ. Sci. 2021, 14, 3160.

[3] Y. Wu, W. Wei, R. Yu, L. Xia, X. Hong, J. Zhu, J. Li, L. Lv, W. Chen,Y. Zhao, L. Zhou, L. Mai, Adv. Funct. Mater. 2022, 32, 2110910.

[4] a) M. Bao, I. S. Amiinu, T. Peng, W. Li, S. Liu, Z. Wang, Z. Pu,D. He, Y. Xiong, S. Mu, ACS Energy Lett.2018, 3, 940; b) K. Eiler,S. Suriñach, J. Sort, E. Pellicer, Appl Catal B2020, 265, 118597;c) B. Pang, X. Liu, T. Liu, T. Chen, X. Shen, W. Zhang, S. Wang,T. Liu, D. Liu, T. Ding, Z. Liao, Y. Li, C. Liang, T. Yao, Energy Environ.Sci. 2022, 15, 102.

[5] a) L. Gao, Z. Yang, T. Sun, X. Tan, W. Lai, M. Li, J. Kim,Y. F. Lu, S. I. Choi, W. Zhang, C. Ma, S. C. Smith, Y. G. Zhou,H. Huang, Adv. Energy Mater. 2022, 12, 2103943; b) D. Kobayashi,H. Kobayashi, D. Wu, S. Okazoe, K. Kusada, T. Yamamoto,T. Toriyama, S. Matsumura, S. Kawaguchi, Y. Kubota, S. M. Aspera,H. Nakanishi, S. Arai, H. Kitagawa, J. Am. Chem. Soc.2020, 142,17250.

[6] P. Zhou, X. Lv, D. Xing, F. Ma, Y. Liu, Z. Wang, P. Wang, Z. Zheng,Y. Dai, B. Huang, Appl Catal B 2020, 263, 118330.

[7] T. Zhao, X. Shen, Y. Wang, R. K. Hocking, Y. Li, C. Rong,K. Dastafkan, Z. Su, C. Zhao, Adv. Funct. Mater.2021, 31,2100614.

[8] L. Peng, J. Shen, L. Zhang, Y. Wang, R. Xiang, J. Li, L. Li, Z. Wei,J. Mater. Chem. A 2017, 5, 23028.

[9] H. Xu, J. Wan, H. Zhang, L. Fang, L. Liu, Z. Huang, J. Li, X. Gu,Y. Wang, Adv. Energy Mater. 2018, 8, 1800575.

[10] a) S.-Y. Ang, D. A. Walsh, Appl. Catal. B 2010, 98, 49; b) L.-W. Chen,X. Guo, R.-Y. Shao, Q.-Q. Yan, L.-L. Zhang, Q.-X. Li, H.-W. Liang,Nano Energy 2021, 81, 105636.

[11] a) S. C. Purdy, P. Ghanekar, G. Mitchell, A. J. Kropf, D. Y. Zemlyanov,Y. Ren, F. Ribeiro, W. N. Delgass, J. Greeley, J. T. Miller, ACSAppl. Energy Mater. 2020, 3, 1410; b) Z. Cui, H. Chen, M. Zhao,D. Marshall, Y. Yu, H. Abruna, F. J. DiSalvo, J. Am. Chem. Soc. 2014,136, 10206.

[12] a) R. Jiang, Y. Da, X. Han, Y. Chen, Y. Deng, W. Hu, Cell Rep. Phys.Sci. 2021, 2, 100302; b) R. Jiang, Y. Da, J. Zhang, H. Wu, B. Fan,J. Li, J. Wang, Y. Deng, X. Han, W. Hu,Appl. Catal. B 2022, 316,121682.

[13] K. Fan, Y. Ji, H. Zou, J. Zhang, B. Zhu, H. Chen, Q. Daniel, Y. Luo,J. Yu, L. Sun, Angew. Chem., Int. Ed. 2017, 56, 3289.

[14] K. Fan, H. Zou, L. Duan, L. Sun, Adv. Energy Mater.2020, 10,1903571.

[15] a) D. Liu, X. Li, S. Chen, H. Yan, C. Wang, C. Wu, Y. A. Haleem,S. Duan, J. Lu, B. Ge, P. M. Ajayan, Y. Luo, J. Jiang, L. Song,Nat. Energy 2019, 4, 512; b) Z. Li, W. Niu, Z. Yang, N. Zaman,W. Samarakoon, M. Wang, A. Kara, M. Lucero, M. V. Vyas, H. Cao

H. Zhou, G. E. Sterbinsky, Z. Feng, Y. Du, Y. Yang, Energy Environ.Sci. 2020, 13, 884; c) N. Nie, D. Zhang, Z. Wang, Y. Qin, X. Zhai,B. Yang, J. Lai, L. Wang, Small 2021, 17, e2102879.

[16] I. Jang, S. Lee, E. Lee, D.-W. Lee, H.-Y. Park, B. B. Choi, H. C. Ham,S. J. Yoo, Nano Today 2021, 41, 101316.

[17] a) H. Huang, K. Li, Z. Chen, L. Luo, Y. Gu, D. Zhang, C. Ma,R. Si, J. Yang, Z. Peng, J. Zeng,J. Am. Chem. Soc. 2017, 139, 8152;b) L. Gao, T. Sun, X. Tan, M. Liu, F. Xue, B. Wang,

J. Zhang, Y.-F. Lu,C. Ma, H. Tian, S. Yang, S. C. Smith, H. Huang, Appl. Catal. B 2022,303, 120918.Adv. Energy Mater. 2023, 13, 2300127